INSTITUTE OF PHYSICS PUBLISHING NANOTECHNOLOGY

Nanotechnology **16** (2005) 1–6 doi:10.1088/0957-4484/16/0/000

Molecular nano-junctions formed with different metallic electrodes

Nikolai B Zhitenev[1,3], Artur Erbe[1,4], Zhenan Bao[1,5], Weirong Jiang[1,2] and Eric Garfunkel[2]

[1] Bell Labs, Lucent Technologies, Murray Hill, NJ 07974, USA
[2] Department of Chemistry, Rutgers University, Piscataway, NJ 08854, USA

E-mail: zhiten@lucent.com

Received 29 September 2004, in final form 29 November 2004
Published
Online at stacks.iop.org/Nano/16/1

Abstract

Conductance of nanoscale junctions consisting of a molecular monolayer in contact with different metal electrodes is studied. The characteristic energy scales of conductance are determined from the temperature dependence and from the non-linear current–voltage characteristics. Conductance measured at small bias follows Arrhenius behaviour. The effective activation energies are dependent on the metal contacts. The activation energies, typically in the range of 5–150 meV, are small compared to the expected molecular energy level spacings. The nature of the low-energy states remains unclear; however, some mechanisms, such as doping of the molecular layer by metal atoms, can be excluded. For certain metal pairs, the energies extracted from the onset of the non-linearity correspond to the low-bias activation energies, while for other metals this is not observed. These differences are probably caused by the differences in the relative topography of metal electrodes defining the effective conducting paths through the molecular layer.

1. Introduction

One of the main goals of molecular electronics is to bring the vast capabilities of synthetic chemistry into the realm of nanoelectronic devices. A variety of advanced techniques have been exploited to fabricate device-like structures based on a single molecule or on a small number of molecules. Some interesting effects have been reported, including negative differential conductance [1], Coulomb blockade and the Kondo effects on single molecules [2, 3], and bistable molecular devices [4, 5]. Despite these and other exciting results, a consistent understanding has yet to emerge. Not surprisingly, the electronic properties of devices at such a length scale are sensitive to the microscopic configuration of all essential device constituents including the organic molecules and the metal electrodes, as well as other desired or undesired dopants and defects [5, 6].

Recently, we have observed that the apparent conductance mechanism though molecular junctions is affected by the surface topography and the metal contacts [6]. Here, we systematically study self-assembled monolayers (SAMs) in contact with a variety of metals. The metals range from noble metals that weakly interact with organics [7] to metals that are expected to react strongly with organics to conductive metal oxides. Each combination of metal contacts displays reproducible and unique transport properties. However, the characteristic energy scale of conductance is below 150 meV for all studied contact combinations. These energies are small compared to the expected molecular energy level spacings. The possibility that the low-energy states mediating the transport are created by metal atom doping is unlikely considering the wide range of exploited metal reactivity. The states exist in monolayers created by interaction between molecules, by disorder or by other dopants. Other differences in transport behaviour can be associated with different relative surface topography of the metals.

2. Experimental details

2.1. Tips as templates for nano-junctions

Molecular junctions of a few nanometres in size are fabricated on sharp quartz tips [6, 8]. The pyramid-shaped tips are pulled

[3] Author to whom any correspondence should be addressed.
[4] Present address: Fachbereich Physik, Universität Konstanz, 78464 Konstanz, Germany.
[5] Present address: Department of Chemical Engineering, Stanford University, Stanford, CA 94305, USA.

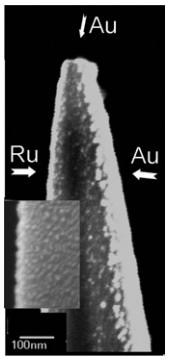

Figure 1. The junctions are made on sharp ends of pulled rods with square cross sections. The scheme shows an SEM image of a tip with Ru–T3–Au junctions. First, Ru is evaporated from the left side and the molecular layer is assembled. Next, the Au electrode is evaporated on the face of the tip opposite the Ru electrode. Finally, Au is evaporated from the tip side connecting the Ru electrode with the molecules and the Au electrode. At the typical thickness of the last evaporation <3–4 nm, continuous Au film does not form on top of the monolayer on the slanted face of the tip. The inset shows an SEM image of Au clusters accumulated on top of the Ru electrode with the SAM.

from 1×1 mm^2 cross section quartz rods with a micropipette puller reproducibly yielding 20–30 nm sharp ends. The metal electrodes are evaporated on opposite faces of the rods in three steps (figure 1). First, contact pads are evaporated ∼1 mm away from the tip and contact wires are soldered. Second, the drain electrode is evaporated on one face of the sharpened rod and a molecular layer is assembled on this electrode. Last, the rod with the SAM is placed in a vacuum evaporator. The source electrode is evaporated on the face opposing the drain. Then, the rod is rotated so that the tip faces the evaporation target. The final evaporation of a thin metal film connects the source with the drain electrode covered by the SAM. Due to the difference in the incident angle, the accumulated metal is thicker on the tip than on the slanted faces of the rod. The overall thickness is chosen such that a continuous metal film on top of the SAM is formed only in the immediate vicinity of the tip. Figure 1 shows disconnected Au clusters accumulated after the final evaporation on top of the slanted part of the drain with the SAM.

The choice of fused quartz as tip material as opposed to other common glasses is dictated by its relative hardness. Pulled quartz tips form the sharpest ends down to 15 nm size, and the pulling procedure can be tuned to reproducibly yield duller ends [6]. Additionally, we found that sharp tips, especially hollow inside, made from softer borosilicate and aluminosilicate glasses could be deformed by stresses arising during evaporation of certain metals. The square cross section of the rods is essential in avoiding undesired electrical connections between the electrodes. Typically, no conductance between the source and the drain is detected before the final metal evaporation onto the tip.

The molecule used in this work is terthiophene (T3) terminated with thiol bonding groups at both ends. Thiol terminations are commonly used to link organics to gold [9]. The assembly of this molecule has been generally characterized in [10]. STM images of conjugated dithiol molecules do not display the high degree of order common for alkanethiols. A typical STM image of a T3 monolayer

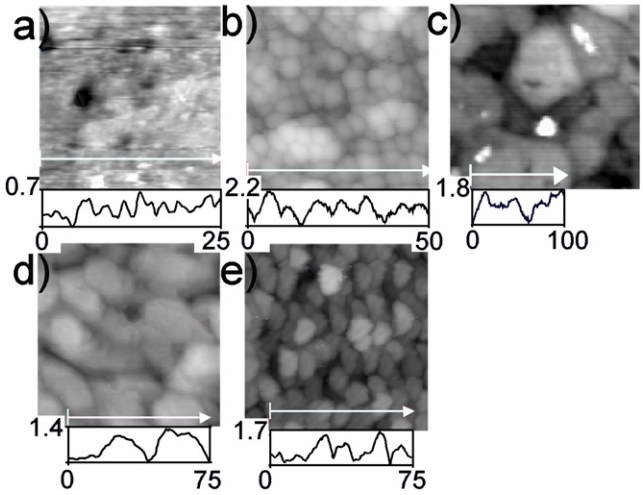

Figure 2. Different sources of disorder in molecular junctions. (a) STM image of a T3 layer assembled on flat Au on a mica substrate. Dark spots are depressions associated with Au surface modification caused by the SAM. The layer appears rather disordered compared to common alkanethiol SAMs. The intermittent interaction between the STM tip and the top thiol termination of the T3 SAM is one of the main reasons for the lower quality of the images. (b) Au clusters on top of a T3 monolayer. ∼1 nm of Au is evaporated on top of T3. The visible roughness is ∼2 nm, the size of clusters ∼3–5 nm. The visible height contrast is a combination of the topography and the conductance of differently bonded clusters. (c) ∼2 nm of Ti evaporated on top of T3 SAM assemble on Au on mica. Comparing to Au top film, the metal layer is significantly smoother. The grain structure is similar to the underlying Au surface. (d) Thermally evaporated 20 nm Au film on top of SiO_2. Grain size 25 nm, rms roughness 0.4 nm. (e) Electron-beam evaporated 20 nm Ru film on top of SiO_2. Grain size 8 nm, rms roughness 0.5 nm.

assembled on Au/mica is shown in figure 2(a). The visible topography is rather flat, and the corrugations are smaller than the molecular length. Usually, the images suffer from intermittent strong interactions between the top thiol molecular terminations and the scanning tip, and do not represent the real topography of the monolayer. Figure 2(b) shows an STM image of a ∼1 nm Au film deposited on top of a T3 monolayer. The monolayers of conjugated dithiols impede penetration of incident metal atoms more effectively than better ordered monolayers of alkane thiols [11].

After evaporation of the contact pads, eight samples are wired and processed as a single batch. Immediately after the evaporation of the drain electrodes, the SAMs are assembled on the drain electrodes. The tips are soaked in a tetrahydrofuran (THF) solution of T3 (about 0.01 mM), with a few drops of 37% aqueous solution of ammonium hydroxide added for *in situ* deprotection of thioacetyl groups, at room temperature for 5–30 min, then rinsed with THF, acetone and isopropanol. As a function of soaking time (t_s), no qualitative difference was observed either in electrical properties of the junctions (5 min $< t_s <$ 1 h) or in STM images (5 min $< t_s <$ 24 h). After the SAM formation, the samples are placed back in the vacuum evaporator.

2.2. Choice of metallic electrodes

To study the interaction between the SAM and the contacts we have chosen materials with widely different chemical

properties. Au is a common electrode material in electronics because of its chemical stability in air. Most other metals form oxides that can affect the conductance of the junctions. For example, junctions made with reactive top contacts such as Al and Cr become quite resistive upon oxidation in air. The thickness and resistance of the oxide vary from case to case and do not scale with the heat of formation of the oxide. Pd and Ag are more reactive than Au and are slightly oxidized in air. Ru and Ti react strongly with organics [11, 12] and are readily oxidized. However, their oxides are conductive and ∼50% of fabricated samples display measurable conductance. Pd and Ru have been also used as bottom electrodes. Ion scattering shows that a thin oxide film (10–20 Å) is formed on top of e-beam evaporated Ru once brought to air. The Ru oxide is conductive, and this is confirmed in our case by fabricating Ru/RuO–Au junctions without molecules.

Most of the metals have been thermally evaporated. The conductance of two samples is monitored during the evaporation. Typically, the final metal evaporation from the tip side is stopped when conductance of the order of 10^{-7}–10^{-5} Ω^{-1} is detected on the control samples. The character of the conductance growth during the evaporation as a function of metal thickness varies with the type of metal used for the contacts. In the case of junctions assembled on Au and Pd the conductance increases mainly in sudden jumps, occasionally developing shorts between the contacts. Immediately after evaporation, the conductance usually decreases in a step-like manner. The conductance decrease is observed in vacuum (10^{-6} Torr), in air and in helium atmosphere at 300 K. The junctions become stable at temperature below 200–250 K. The jumpy relaxation is probably related to metal diffusion and crystallization and/or atomic movements at the metal–molecule interfaces. All fabricated junctions are electrically tested. The junctions are kept electrically grounded during handling to avoid junction damage or modification by a static discharge. The rejected junctions are the shorted ones with resistance indistinguishable from the contact lead resistance and extremely resistive junctions (>20 GΩ@300 K). The yield of junctions can be as high as 70% for Au–T3–Au junctions. The yield of junctions assembled on Pd is noticeably lower than for Au electrodes (∼20–30%). The junctions assembled on Ru display more regular conductance increase during the top metal evaporation. Very few junctions are shorted while about ∼50% are too resistive for the measurements. The Ru/RuO-assembled junctions are relatively stable in air after the fabrication and initial oxidation. In particular, Ru–T3–Au and Ru–T3–Ru junctions change only slightly in conductance after a few days in air. Ru–T3–Ag and Ru–T3–Pd and especially Ru–T3–Ti junctions are less stable because of the oxidation of the top electrode. Ti and Ru top contacts are deposited by e-beam evaporation without conductance monitoring.

2.3. Disorder in molecular junctions

The features in images shown in figure 2 illustrate the length scales and the sources of disorder present in metal–molecule–metal junctions. The first scale is related to the defects and imperfections of the molecular packing. The features in figure 2(a) are produced by packing defects and are affected by intermittent tip–molecule interaction. The second scale is associated with upper interface formation (figures 2(b) and (c)). The growth of metal film deposited by evaporation is a complicated kinetic process dependent on the bond strength of the metal to various surface sites, sticking probability, mobility of metal atoms on top of the SAM and diffusion through the SAM. The morphology of the top metal electrode is unique for every combination of a particular SAM and type of metal. The third scale is the granularity and the topography of the bottom metal electrode used for the assembly. Figures 2(d) and (e) show the STM images of two common substrates (Au and Ru/RuO) used in the present experiment. The length scale of the defects associated with the substrate is larger in this case than the first two scales. Earlier, we established that the ratio between the grain size and the size of the junction plays an important role in the apparent conductance mechanism [6]. The current research is limited to the smallest junction size that is less than or comparable with the grain size.

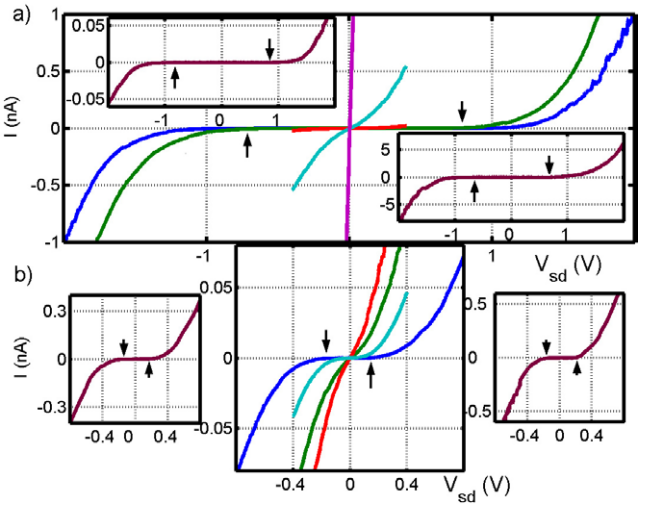

Figure 3. Typical I–V curves at different temperatures for various metal–T3–metal junctions. (a) Ru–T3–Ru junctions. I–V curves are measured at $T = 240$, 110, 55, 22 and 4.2 K. (b) Au–T3–Ag junctions. I–V curves are measured at $T = 240$, 190, 90 and 4.2 K. Insets show the typical reproducibility of the non-linear onset of conductance for different samples made within the same processing batch. All I–V curves are taken at $T = 4.2$ K. While the conductance can vary significantly, the onset of the tunnelling conductance shown by arrows is reasonably reproducible.

(This figure is in colour only in the electronic version)

3. Results

Figure 3 shows representative current–voltage curves measured on some molecular junctions. Conductance (σ_0 defined as $(\mathrm{d}I/\mathrm{d}V_{\mathrm{sd}})$ at $V_{\mathrm{sd}} = 0$) is strongly dependent on temperature and vanishes at low temperatures. The size of the conductance gap seen in low-temperature I–V curves is quite reproducible and characteristic of a particular combination of metal contacts. Low-temperature I–V curves measured on the junctions prepared within the same processing batch are shown in insets to figures 3(a) and (b). The onset of the conductance V_{on} at finite V_{sd} is not always sharp. Values of V_{on} determined as V_{sd} corresponding to current level of 0.1 pA as shown in figure 3 vary less than 50% for a given combination of metals.

Table 1. Activation energy E_a (meV), ratio eV_{on}/E_a and number of measured samples of various metal–T3–metal junctions. The number of samples displaying different conductance mechanisms is shown in parenthesis.

	Source				
Drain	Au	Pd	Ag	Ru/RuO	Ti
Au	3.6–18/... 26/(2)	65–125/2–4 8/(0)	25–40/3–5 6/(0)		
Pd	60–90/2–4 7/(1)	30–45/3–5 3/(1)			
Ru/RuO	9–25/25–50 7/(0)	30–45/3–5 4/(1)		35–70/13–20 10/(0)	25–50/3–5 4/(0)

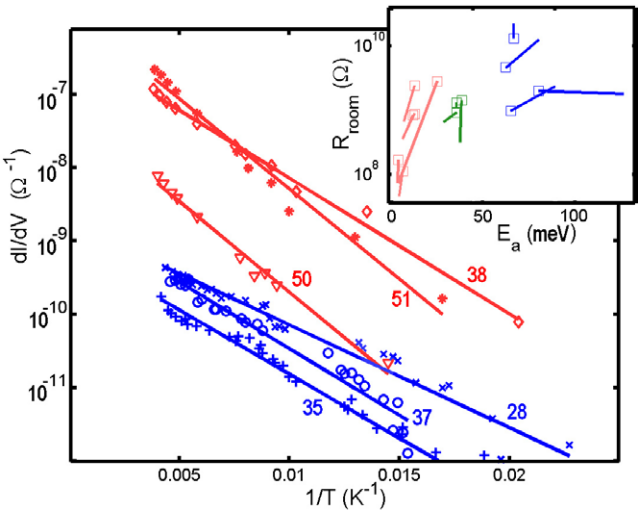

Figure 4. Activation energies for Ru–T3–Ru (red) and Au–T3–Ag (blue) metal–molecule junctions. Three samples from a single batch of tips are shown in each case to illustrate the typical variation. Inset: change of room-temperature resistance and activation energy observed for Au–T3–Au (red), Au–T3–Ag (green) and Au–T3–Pd (blue) after two days in vacuum at $T \sim 300$ K. Squares mark the final states. Conductance changes substantially, reflecting modifications in the microscopic structure of the junctions. However, activation energies remain in the same range.

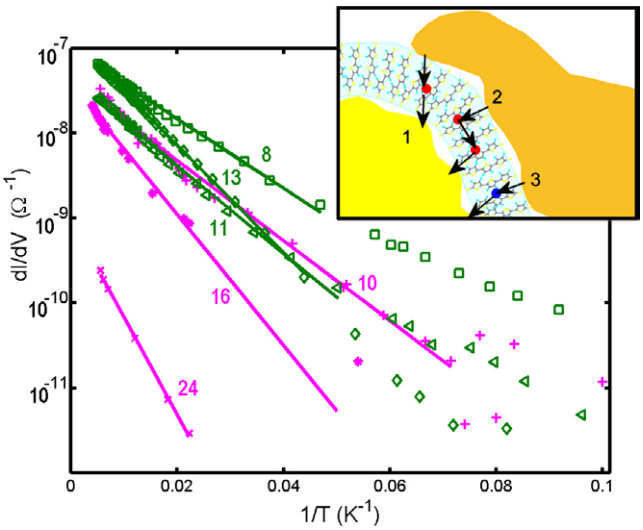

Figure 5. Activation energies for Au–T3–Au (green) and Ru–T3–Au (purple) metal–molecule junctions. Three samples from the same batch of tips are shown in each case to illustrate the typical variation. Inset: possible conductance channels observed in junctions of different type. Tunnelling path 1 designates the sequential tunnelling through the low-energy state dominating the conductance for Au–T3–Ag, Au–T3–Pd, Ru–T3–Pd and Ru–T3–Ti electrodes. Path 2 illustrates in-layer hopping conductance observed in Au–T3–Au and Ru–T3–Au at small V_{sd}. Path 3 is sequential tunnelling through the higher-energy state determining the conductance of Ru–T3–Ru junctions at large applied bias V_{sd}.

Figure 4 shows that the temperature dependence of σ_0 is another characteristic of the junctions made with particular metal contacts. Interestingly, the junctions Ru–T3–Ru and Au–T3–Ag shown in figure 3 display markedly different onset voltages V_{on} at low temperature but demonstrate quite similar temperature dependence at zero bias. The characteristic energy scale is determined by fitting the temperature dependence with the Arrhenius law. For junctions with Au top contacts, the activation energies, E_a, are particularly small as shown in figure 5 for Au–T3–Au and Ru–T3–Au junctions. The determined E_a is in the range of 3.6–125 meV for all studied junctions. The characteristic activation energy, the threshold voltage and the number of measured samples for different electrode pairs are summarized in table 1. A small number of fabricated junctions (table 1) display a different character of conductance. In these cases, σ_0 does not vanish at low temperature and the overall temperature dependence is rather weak.

As mentioned above, most of the junctions change during the fabrication and following the fabrication in vacuum and in air. The initial characterization of conductance mechanisms inside the evaporator chamber is rather incomplete. The present set-up does not allow for I–V measurements in a broad temperature range. The meaningful range of V_{sd} is limited to ∼100–600 mV at room temperature because of frequent voltage-induced switching events. Most of the studied junctions display nearly linear I–V curves in this voltage range at 300 K. However, the values of V_{on} determined for a number of junctions generally agree with the values of V_{on} measured after the air exposure.

To additionally understand how the junction ageing affects the conductance mechanism, we have monitored a few junctions over an extended period of time, intentionally allowing further changes of conductance. The inset to figure 4 shows resistances at room temperature and activation energies immediately after the preparation and after ageing for two days at room temperature in vacuum. Both the absolute value of conductance and the activation energy typically change. The character of these changes is specific for a particular contact combination. For Au–T3–Au junctions the conductance always decreases and the activation energy increases after ageing. For Au–T3–Pd junctions, the activation

energy typically decreases. However, this further ageing does not change the general features of the conductance or its overall temperature dependent character.

4. Discussion

A common way to analyse molecular junctions starts with calculation of conductance of isolated molecules that are strongly or weakly connected to metal contacts. The calculated tunnelling conductance [9, 13] of short conjugated molecules connected to metals through the sulfur bonds is in the range of 10^{-6}–10^{-8} Ω^{-1}. The conductance mechanism is tunnelling with weak temperature dependence. While the room temperature conductance of the junctions falls within this range, the conductance vanishes at low T. The observed temperature dependence is inconsistent with this model [9, 13], implying absence of good chemical bonds between the SAM molecules and the contacts in our junctions. Other theoretical models allow for arbitrarily weak coupling between the molecules and the contacts [9, 14]. In these models, the conductance is the sequential tunnelling through discrete molecular states, only slightly modified by small overlap with the metal states. The conductance in this case displays an activated temperature dependence. The energy scale is the difference between the molecular energy levels and the Fermi level of the metal contact. The optical bandgap of the T3 molecule of 2.8 eV [10] can be used as an estimate for the energy spacing between the highest occupied and the lowest unoccupied molecular levels. The experimentally determined activation energies (smaller than 150 meV) would correspond within this model to very close alignment of key molecular orbitals with the metal Fermi level. Considering the broad range of studied metal contacts and their very different work functions, an accidental alignment is unlikely.

Clearly the conductance of the junctions cannot be explained within an idealized single-molecule approximation. The alignment of the molecular states relative to the metal Fermi level can be substantially affected either by a strong variation of interfacial dipoles or by unintentional doping [15–17]. A possible source of doping can be metal atoms penetrating the SAM during evaporation of the second contact. Au forms bonds with thiols but only weakly interacts with thiophene and may present states slightly above or below the metal Fermi level [18–20]. Ag and Pd react more strongly with sulfur on thiophene rings [18, 21]. Finally, Ti is known to strongly react with organics [11, 12, 21, 22], forming carbides. The electronic states resulting from these reactions can differ by a few eV in energy. In the experiment, all activation energies are small.

The energy levels could be associated with defects in the SAM and unintentional doping [15–17]. The defects of similar energy have been observed in other nanoscale molecular devices [23, 24], thin organic films [25, 26] and organic crystals [27, 28]. The nature of these defects is not reliably established. The defect energy is close to other energy scales such as the lowest energies of intramolecular vibrations, intermolecular vibrations and electronic overlap in molecular crystals.

The key characteristic of conductance through molecules is the effective coupling between states in the SAM and the metal contacts. In the absence of good coupling to the molecular states, the states with the lower energy provide a better conducting pathway. The geometry of the most conductive path depends on the surface topography of the metal–molecule interface and on the relative topography of the metal contacts. The strongly varying ratio between the activation energy at zero bias and the threshold voltage V_{on} indicates a very different geometry of the conducting pathway for different combinations of metals. In the usual model of sequential tunnelling, the Fermi level of one of the metal contacts lines up with the energy level of an intermediate state at an applied source–drain V_{on}, opening an effective conductance channel. The ratio eV_{on}/E_a equals two for symmetric junctions. A large group of junctions in our work, including Au–T3–Ag, Au–T3–Pd and Ru–T3–Pd and Ru–T3–Ti, display an eV_{on}/E_a ratio in the range of two to five, consistent with the sequential tunnelling model (figure 5(b), path 1). However, the ratio is much larger, ∼15–30, for Ru–T3–Ru and Ru–T3–Au junctions. In the case of Au–T3–Au the ratio is very large and poorly reproducible. We suggest that in these junctions the conducting pathway at small bias involves sequential hops within the SAM layer (figure 5(b), path 2). An electric field applied between the contacts affects the rate of such hops substantially less than the rate of hops in the field direction. The in-plane hops are the limiting steps resulting in a temperature-dependent rate at $V_{sd} \gg 2E_a/e$. The onset voltage is not well defined in this model, consistent with results on Au–T3–Au junctions. The reproducible V_{on} in Ru/RuO-assembled junctions is possibly associated with the tunnelling through electronic states of different origin with markedly larger energy at 0.5 eV (figure 5(b), path 3). The states of this energy might be the molecular states or hybridized molecular–metal states.

The peculiarities of coupling and the unusual geometry of conducting pathways typical for junctions with Au overlayer correlate with the observed roughness of interfaces. Au evaporated on top of the SAM forms grainy surfaces shown in figure 2(b) with a small percentage of bonding sites. The conducting path through the SAM is ill defined in this case. Other metals form smoother overlayers (figure 2(c)) and the relation between V_{on} and E_a is closer to the characteristics of conventional tunnelling devices.

In summary, we investigated conductance of molecular junctions in contact with a variety of different metals. The main conductance channel is hopping with a characteristic energy scale determined by the combination of metals. The energy is small compared to the energy spacing expected for accessing molecular states in SAM. Based on our results we can exclude doping of the SAM by penetrating metal atoms. The low-energy states in SAM are probably related to defects or unintentional doping by impurities. The differences in transport behaviour of different metal contacts are associated with the topography of metal–molecule interfaces and coupling to the defects and molecular states.

Acknowledgments

We would like to acknowledge useful discussions with V Fal'ko, E Chandross, C Nuckolls and M Steigerwald.

References

[1] Chen J, Reed M A, Rawlett A M and Tour J M 1999 Large on–off ratios and negative differential resistance in a molecular electronic device *Science* **286** 1550

[2] Park J *et al* 2002 Coulomb blockade and the Kondo effect in single-atom transistors *Nature* **417** 722

[3] Liang W, Shores M P, Bockrath M, Long J R and Park H 2002 Kondo resonance in a single-molecule transistor *Nature* **417** 725

[4] Collier C P, Mattersteig G, Wong E W, Luo Y, Beverly K, Sampaio J, Raymo F M, Stoddart J F and Heath J R 2000 A [2]catenane-based solid state electronically reconfigurable switch *Science* **289** 1172

[5] Stewart D R, Ohlberg D A A, Beck P A, Chen Y, Williams R S, Jeppesen J O, Nielsen K A and Stoddart J F 2004 Molecule-independent electrical switching in Pt/organic monolayer/Ti devices *Nano Lett.* **4** 133

[6] Zhitenev N B, Erbe A and Bao Z 2004 Single- and multigrain nanojunctions with a self-assembled monolayer of conjugated molecules *Phys. Rev. Lett.* **92** 186805

[7] Beebe J M, Engelkes V B, Miller L L and Frisbie C D 2002 Contact resistance in metal–molecule–metal junctions based on aliphatic SAMs: effects of surface linker and metal work function *J. Am. Chem. Soc.* **124** 11268

[8] Zhitenev N B, Meng H and Bao Z 2002 Conductance of small molecular junctions *Phys. Rev. Lett.* **88** 226801

[9] Kergueris C, Bourgoin J P, Palacin S, Esteve D, Urbina C, Magoga M and Joachim C 1999 Electron transport through a metal–molecule–metal junction *Phys. Rev.* B **59** 12505

[10] Boer B d, Meng H, Perepichka D F, Zheng J, Frank M M, Chabal Y J and Bao Z 2003 Synthesis and characterization of conjugated mono- and dithiol oligomers and characterization of their self-assembled monolayers *Langmuir* **19** 4272

[11] Boer B d, Frank M M, Chabal Y J, Jiang W, Garfunkel E and Bao Z 2004 Metallic contact formation for molecular electronics: interactions between vapor-deposited metals and self-assembled monolayers of conjugated mono- and dithiols *Langmuir* **20** 1539

[12] Walker A V, Tighe T B, Stapleton J, Haynie B C, Upilli S, Allara D L and Winograd N 2004 Interaction of vapor-deposited Ti and Au with molecular wires *Appl. Phys. Lett.* **84** 4008

[13] Heurich J, Cuevas J C, Wenzel W and Schon G 2002 Electrical transport through single-molecule junctions: from molecular orbitals to conduction channels *Phys. Rev. Lett.* **88** 256803

[14] Hettler M H, Schoeller H and Wenzel W 2002 Non-linear transport through a molecular nanojunction *Europhys. Lett.* **57** 571

[15] Yang Z, Lang N D and Ventra M D 2003 Effects of geometry and doping on the operation of molecular transistors *Appl. Phys. Lett.* **82** 1938

[16] Mehrez H, Wlasenko A, Larade B, Taylor J, Grütter P and Guo H 2002 I–V characteristics and differential conductance fluctuations of Au nanowires *Phys. Rev.* B **65** 195419

[17] Lang N D and Avouris P 2003 Understanding the variation of the electrostatic potential along a biased molecular wire *Nano Lett.* **3** 737

[18] Lachkar A, Selmani A, Sacher E, Leclerc M and Mokhliss R 1994 Metallization of polythiophenes. 1. Interaction of vapor-deposited Cu, Ag and Au with poly(3-hexylthiophene) (P3HT) *Synth. Met.* **66** 209

[19] Noh J, Ito E, Nakajima K, Kim J, Lee H and Hara M 2002 High-resolution STM and XPS studies of thiophene self-assembled monolayers on Au(111) *J. Phys. Chem.* B **106** 7139

[20] Larade B and Bratkovsky A 2004 Effect of impurities on transport through organic molecular films from first principles *Preprint* cond-mat/0408043

[21] Elfeninat F, Fredriksson C, Sacher E and Selmani A 1995 A theoretical investigation of the interactions between thiophene and vanadium, chromium, copper, and gold *J. Chem. Phys.* **102** 6153

[22] Lachkar A, Selmani A and Sacher E 1995 Metallization of polythiophenes. 2. interaction of vapor-deposited Cr, V and Ti with poly(3-hexylthiophene) (P3HT) *Synth. Met.* **71** 73

[23] Zhou C, Deshpande M R, Reed M A, Jones L and Tour J M 1997 Nanoscale metal/self-assembled monolayer/metal heterostructures *Appl. Phys. Lett.* **71** 611

[24] Kubatkin S, Danilov A, Hjort M, Cornil J, Bredas J-L, Stuhr-Hansen N, Hedegard P and Bjornholm T 2003 Single-electron transistor of a single organic molecule with access to several redox states *Nature* **425** 698

[25] Chesterfield R J, McKeen J C, Newman C R, Frisbie C D, Ewbank P C, Mann K R and Miller L L 2004 Variable temperature film and contact resistance measurements on operating n-channel organic thin film transistors *J. Appl. Phys.* **95** 6396

[26] Knipp D, Street R A and Volkel A R 2003 Morphology and electronic transport of polycrystalline pentacene thin-film transistors *Appl. Phys. Lett.* **82** 3907

[27] Butko V Y, Chi X, Lang D V and Ramirez A P 2003 Field-effect transistor on pentacene single crystal *Appl. Phys. Lett.* **83** 4773

[28] Minari T, Nemoto T and Isoda S 2004 Fabrication and characterization of single-grain organic field-effect transistor of pentacene *J. Appl. Phys.* **96** 769